MRI Intensity Inhomogeneity Correction by Minimizing Joint Information of Intensity and Space*

LIU Chang-chun[1], HU Shun-bo[1,2], GU Jian-jun[1,3], YANG Jin-bao[1]

(1 *School of Control Science and Engineering, Shandong University, Ji'nan* 250061, *China*)

(2 *Department of Physics, Linyi Normal University, Linyi* 276005, *China*)

(3 *Department of Electrical and Computer Engineering, Dalhousie University, Hallfax, NS B3J2X4, Canada*)

Abstract: In the intensity inhomogeneity correction of magnetic resonance imaging, since entropy minimization method did not consider space information, a better correction method based on joint information minimization was proposed, which integrated image intensity features with additional spatial image features. The space features referred to intensity derivatives. The joint entropy between image intensities and corresponding derivatives in a corrupted image is greater than that in an uncorrupted one, and it is calculated by using the joint probability distribution of image intensities and corresponding derivatives. The results on simulated brain images and clinical brain MR images show that joint information minimization method between intensities and their second derivatives is good. It can largely decrease the overlap between white matter and gray matter.

Key words: Image processing; Intensity inhomogeneity correction; Magnetic resonance imaging; Joint information minimization

CLCN: R318 **Document Code**: A **Article ID**: 1004-4213(2007)09-1747-7

0 Introduction

In magnetic resonance imaging (MRI), intensity inhomogeneity reveals intensity variations of the same tissue over the image domain and intensity overlaps in different tissues. Intensity inhomogeneity is also called bias field, intensity nonuniformity, or shading. There are a number of factors that will cause intensity inhomogeneity such as poor radio frequency coil uniformity, static field inhomogeneity, and patient anatomy[1-2]. If quantitative analysis is the final goal, the correction of intensity inhomogeneity is a common preprocessing step in image analysis, for example in segmentation, registration, and quantification.

Researchers have implemented many intensity inhomogeneity correction methods[3-6]. Of those proposed, image smoothing or homomorphic filtering is the most intuitive method, which assumes that intensity inhomogeneity is a low frequency signal which can be removed by applying high pass filters[3,15]. However, this approach often results in blurred edges, and the loss of useful low frequency signals within the same tissues. Li Yin et al. combined the homomorphic filtering and B spline smoothing, improved the correction results[19]. Ref[16] used the distortion model of 3th polynomial to correct CCD image. The nonuniformity correction of infrared focal plane arrays is discussed in reference[17,20]. In ref [18] a new adaptive segmentation method was proposed which estimated the bias field and corrected the intensity inhomogeneities. A retrospective method based on entropy minimization was implemented in [7-9], which assumed that an image corrupted by intensity inhomogeneity contained more information than the corresponding uncorrupted image. They used the parametric polynomial to model the bias field and minimize the information of the acquired images. But they did not consider spatial image features, which were very valuable to intensity inhomogeneity correction.

In this paper a retrospective inhomogeneity correction method is proposed that integrates image intensity features and spatial image features to improve intensity inhomogeneity correction. It is assumed that an image corrupted by intensity inhomogeneity contains more joint information than that of an uncorrupted one. By employing joint entropy minimization between image intensities and corresponding derivatives, a corrected image can be obtained. The new methods using first, second, and third order derivatives were quantitatively evaluated and compared with one recently proposed method[8-9].

*Supported by The Hi-Tech Research and Development Program (863) of China (2006AA02Z4D9) and Shandong Province Nature Science Fundation (Z2006C05)

Tel: 0531-88395384 Email: hsbtiger7748@163.com

Received date: 2007-01-09

1 Method

1.1 Problem formulation

Corruption of intensity homogeneity in MR images can be described by the following degradation model.

$$u(\boldsymbol{x})=v(\boldsymbol{x})s(\boldsymbol{x})+a(\boldsymbol{x}) \tag{1}$$

Where $\boldsymbol{x}$ is a coordinate vector, $u(\boldsymbol{x})$ is a corrupted image, $v(\boldsymbol{x})$ is an uncorrupted true image, $s(\boldsymbol{x})$ is a multiplicative bias field, and $a(\boldsymbol{x})$ is an additive bias field.

Using the degradation model (1), the estimation $\tilde{v}(\boldsymbol{x})$ of the true image $v(\boldsymbol{x})$ is obtained as

$$\tilde{v}(\boldsymbol{x})=u(\boldsymbol{x})\tilde{m}^{-1}(\boldsymbol{x})+\tilde{a}^{-1}(\boldsymbol{x}) \tag{2}$$

where

$$\tilde{m}^{-1}(\boldsymbol{x})=\frac{1}{m(\boldsymbol{x})}=1+\sum_{i=2}^{K}b_i\frac{q_i(\boldsymbol{x})-c_i}{d_i} \tag{3}$$

$$\tilde{a}^{-1}(\boldsymbol{x})=-\frac{a(\boldsymbol{x})}{m(\boldsymbol{x})}=\sum_{i=2}^{K}e_i\frac{q_i(\boldsymbol{x})-f_i}{g_i} \tag{4}$$

The detailed descriptions of the derivation of the expression (3) and (4) are given in[9]. $\tilde{m}^{-1}(\boldsymbol{x})$ and $\tilde{a}^{-1}(\boldsymbol{x})$ are the multiplicative and additive correction components, respectively; b_i and e_i are optimal parameters; c_i, f_i are the neutralization parameters which ensure that the mean intensity values of $\tilde{v}(\boldsymbol{x})$ and $u(\boldsymbol{x})$ will be the same in the domain Ω, which avoids the constant image intensity problem by (joint) entropy minimization. The correction domain Ω contains the tissue data and does not contain the unaffected background (air et al.). d_i and g_i are the normalization parameters which insure that equal change of any optimal parameter will produce the same intensity transformation. $q_i(\boldsymbol{x})$ is the polynomial term which varies with data dimensions and polynomial orders. For example, when $\tilde{m}^{-1}(\boldsymbol{x})$ and $\tilde{a}^{-1}(\boldsymbol{x})$ are modeled by second-order polynomials in a two-dimensional image, $q_i(\boldsymbol{x})$ can be expressed as five polynomial terms: x, y, xy, x^2, y^2. c_i, d_i, f_i, g_i can be written as follows

$$c_i=\sum_{x\in\Omega}u(\boldsymbol{x})q_i(\boldsymbol{x})/\sum_{x\in\Omega}u(\boldsymbol{x}) \tag{5}$$

$$d_i=\frac{1}{N}\sum_{x\in\Omega}|u(\boldsymbol{x})(q_i(\boldsymbol{x})-c_i)| \tag{6}$$

$$f_i=\frac{1}{N}\sum_{x\in\Omega}q_i(\boldsymbol{x}) \tag{7}$$

$$g_i=\frac{1}{N}\sum_{x\in\Omega}|q_i(\boldsymbol{x})-f_i| \tag{8}$$

where $q_2(\boldsymbol{x})=x$, $q_3(\boldsymbol{x})=y$, $q_4(\boldsymbol{x})=xy$, $q_5(\boldsymbol{x})=x^2$, $q_6(\boldsymbol{x})=y^2$, $\boldsymbol{x}=(x,y)$, $i=2,3,4,5,6$. The coordinate origin lies in the center of the image. $N=\sum_{x\in\Omega}1$, is the total pixel's number in domain Ω. The three dimensional version of c_i, d_i, f_i, g_i can be easily derived according to the above two dimensional version.

1.2 Correction strategy

Intensity inhomogeneity causes the dispersion of the intensity distribution in the uncorrupted image, so the joint information contents of the resulting image $u(\boldsymbol{x})$ will be higher than those of the uncorrupted one $v(\boldsymbol{x})$. The optimal parameters $\boldsymbol{b}_o$ and $\boldsymbol{e}_o$ are found by the Powell's method according to the following

$$\{\boldsymbol{b}_o,\boldsymbol{e}_o\}=\arg\min_{\{\boldsymbol{b},\boldsymbol{e}\}}\{JI[v(\boldsymbol{x})]\} \tag{9}$$

Where $\boldsymbol{b}=[b_2,b_3,\cdots,b_K]$, $\boldsymbol{e}=[e_2,e_3,\cdots,e_K]$. JI denotes joint information of $\tilde{v}(\boldsymbol{x})$ and its derivatives. Calculating $\boldsymbol{b}_o$ and $\boldsymbol{e}_o$, then substituting them into (3) and (4) results in $\tilde{m}_o^{-1}(\boldsymbol{x})$ and $\tilde{a}_o^{-1}(\boldsymbol{x})$, respectively, which transforms the acquired image $u(\boldsymbol{x})$ into the optimally corrected image $\tilde{v}_o(\boldsymbol{x})$ according to (2).

1.3 Implementation details

Likar et al. used the parametric polynomial model to minimize the entropy information of the acquired image[9], but the intensity entropy information did not include the spatial image information. Two pixels in different tissues may have the same intensity values, but corresponding second derivatives are different. So using derivatives can reduce cluster overlap and improve inhomogeneity correction. The joint probability distribution between image intensities and its derivatives is calculated firstly using this method, and then its joint entropy is solved. In the uncorrupted true image, the intensity distribution has less overlap, and the intensity values in the same tissue are approximately equal. So the true image derivatives center around 0, and its joint probability distribution centers around a small number of points. Joint entropy of this true image is less than that of the corresponding corrupted one.

The flow chart of the proposed method is shown in Fig. 1.

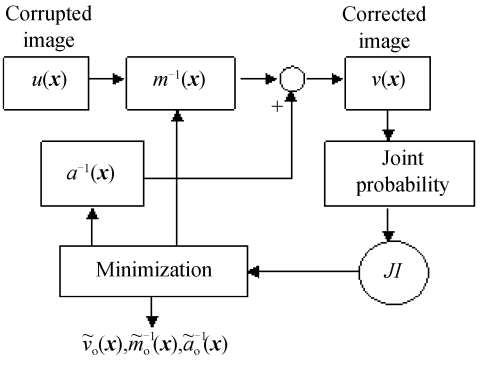

Fig. 1 The flow chart of joint information minimization method

1) Set $\boldsymbol{b}$ and $\boldsymbol{e}$ to a real value vector and calculate $\tilde{v}(\boldsymbol{x})$ according to function (2).

2) Calculate the joint probability distribution $p(.)$ of $\tilde{v}(\boldsymbol{x})$.

3) Calculate the joint entropy $JI[\tilde{v}(\boldsymbol{x})]$.

4) Obtain the optimal $\tilde{v}_o(\boldsymbol{x}), \tilde{m}_o^{-1}(\boldsymbol{x}), \tilde{a}_o^{-1}(\boldsymbol{x})$ using Powell's optimization algorithm.

The joint information JI of image $\tilde{v}(\boldsymbol{x})$ can be quantitatively expressed by joint entropy $H[\tilde{v}(\boldsymbol{x})]$ as

$$JI[\tilde{v}(\boldsymbol{x})]=H[\tilde{v}(\boldsymbol{x})]=-\sum_{m,n}p(m,n)\cdot \log p(m,n) \tag{10}$$

Where $p(m,n)$ is the joint probability, m is the intensity, and n is the derivative of the same pixel in image $\tilde{v}(\boldsymbol{x})$.

The joint entropy is nonnegative and reaches its maximum value when all gray levels are equally likely. Since the estimation image $\tilde{v}(\boldsymbol{x})$ is obtained by an intensity transformation applied to the corresponding corrupted image $u(\boldsymbol{x})$, an integer gray value in a pixel is transformed to a new real value i, which in general lies between two integer values, say k and $k+1$, and the derivative value in that pixel is also transformed to a new real value d, which lies between two integer values, say l and $l+1$. So an intensity interpolation is needed to update the corresponding histogram entries. Partial intensity interpolation is used by which the histogram entries $h(k,l)$, $h(k+1,l)$, $h(k,l+1)$, $h(k+1,l+1)$ are fractionally updated by $(k+1-i)\times(l+1-d)$, $(i-k)\times(l+1-d)$, $(k+1-i)\times(d-l)$, $(i-k)\times(d-l)$, respectively. After the intensity interpolation, the information measure curves become irregular, which will yield less optimal parameters[10-11]. Prior to the calculation of the set of probabilities $p(m,n)$, the histogram $h(m,n)$ is slightly blurred to reduce the effect of imperfect intensity interpolation.

$$h'(m,n)=\leftarrow\sum_{i=-t}^{t}\sum_{j=-t}^{t}h(m+i,n+j)\cdot \min[2t+1-2|i|,2t+1-2|j|] \tag{11}$$

t is set to 2 in this paper. Finally, after normalizing the histogram $h'(m,n)$ the joint probability distribution $p(m,n)$ is obtained. Our experiments use approximately 5 000 image samples, which have been proved to be sufficient to form the 8-bit 1-D histogram that is statistically enough powerful and enables efficient calculation of (joint) entropy[9].

2 Experiments and results

For comparison purposes, four different methods have been tested. Likar's method is named M_1, in which the information similarity measure is entropy. In the second method, named M_2, the information measure is the joint entropy of image intensities and its first derivatives. In the third method, named M_3, the information measure is the joint entropy of image intensities and its second derivatives. In the fourth method, M_4, the information measure is the joint entropy of image intensities and its third derivatives.

2.1 Visual demonstration

In Fig. 2, 2(a) shows an uncorrupted brain tissue image; 2(e) displays the corrupted image by the sine bias field; 2(b) is the joint probability

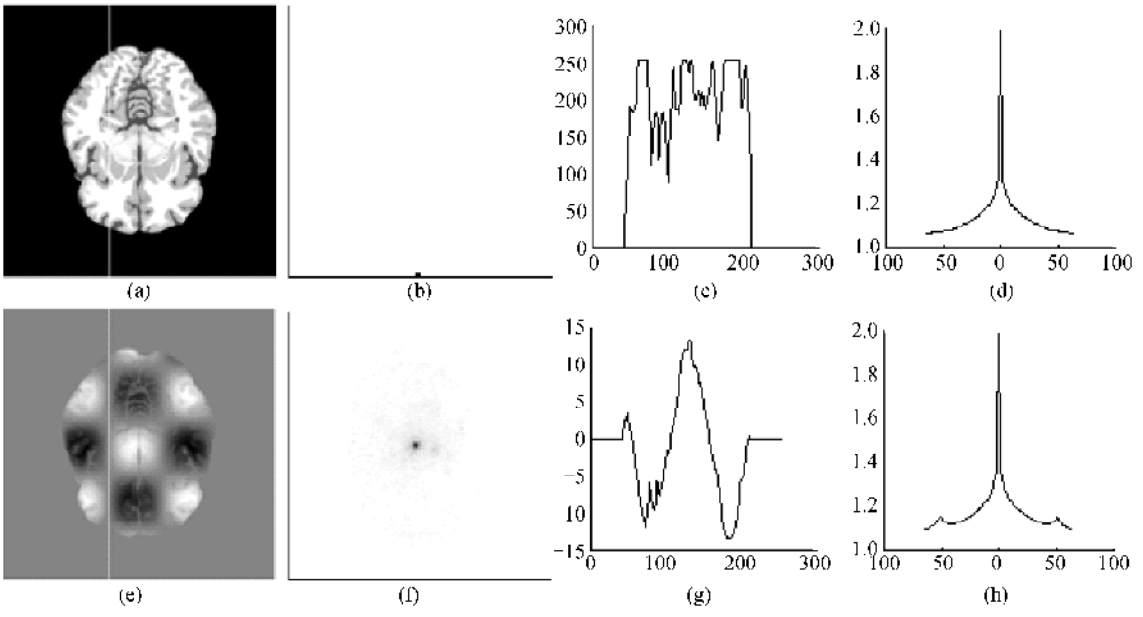

Fig. 2 Influence of intensity inhomogeneity on joint probability distribution, intensity distribution and registration

distribution between 2(a) intensities and its first derivatives; 2(c) is the intensity profile along the vertical white line on 2(a); 2(d) is the curve of the normalized mutual information[12] between 2(a) and its horizontal misalignments; 2(f) is the joint probability distribution between 2(e) intensities and its first derivatives; 2(g) is the intensity profile along the vertical white line illustrated on 2(e); 2(h) is the curve of the normalized mutual information between 2(e) and its horizontal misalignments. In order to show 2(e) clearly, intensity enhancement is used. In 2(b) and 2(f), the horizontal axis corresponds to first derivative values and the vertical axis corresponds to intensity values. The joint probability distribution in 2(f) is more focused than that in 2(b), which implies that the corrupted image by intensity inhomogeneity has greater joint entropy than that of the uncorrupted image. There are more maxima in 2(h) than in 2(d), which indicates that intensity inhomogeneity has bad influence on maximal mutual information registration.

Fig. 3 displays one slice of simulated T_1 volume. In Fig. 3, from (a) to (c) are uncorrected data, corrected data by M_3 method and the additive bias field; From (d) to (f) are the uncorrected data histogram including white matter and gray matter, the corrected data histogram, and the multiplicative bias field. WM is the abbreviation of the withe matter and GM is the abbreviation of the gray matter. The volume histogram illuminates the high contrast between gray matter and white matter. Intensity overlaps between gray matter and white matter reveal intensity inhomogeneity. It should be noted that a part of these overlaps may be caused by intra-tissue variations and part volume effect. The recovery of the histogram can be observed by comparing the histograms of the uncorrected, corrected data. From Fig. 3, it is known that the new method M_3 can largely decrease the intensity overlaps, reduce the spreading of the same tissue distribution, and correct the corrupted image.

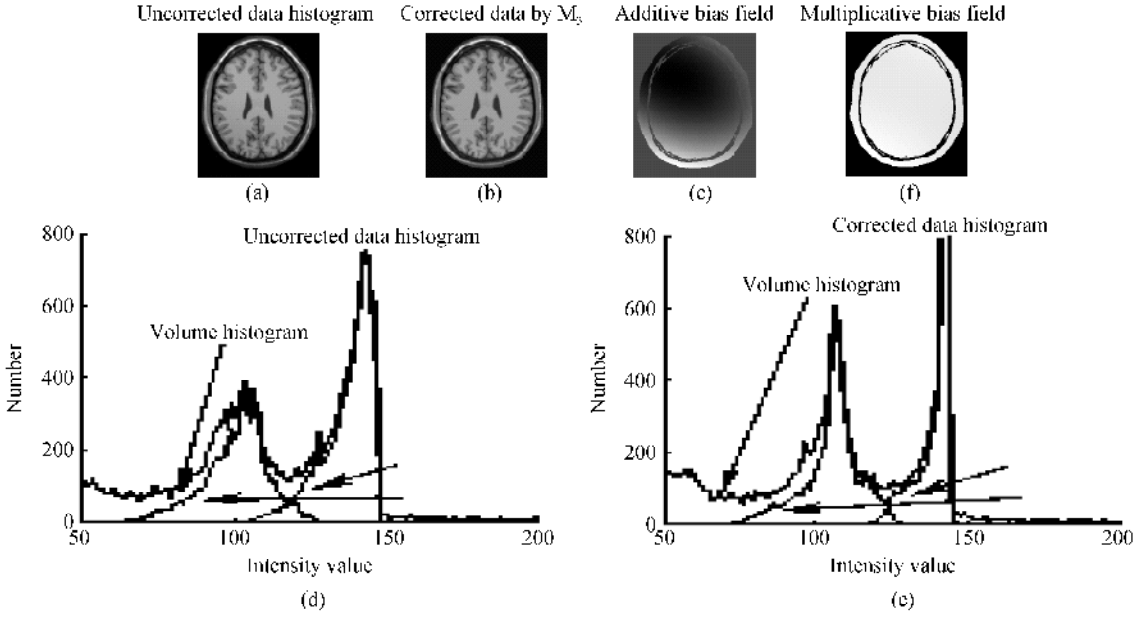

Fig. 3 The bias field correction of T1 data

2.2 Comparison of different methods

In this section, different correction strategies are compared to show that the proposed method could retrospectively correct the intensity variations. In Fig. 4, from (a) to (d) correspond to the curve of uncorrupted images between measured values and optimal parameters; from (e) to (h) correspond to the corrupted images' function between measured values and optimal parameters. The optimal parameters b_i and e_i ($i=2,3,\cdots,6$) were each changed from -20 to 20, with a step of one, and the entropy (or joint entropy) of the transformed image was measured. In Fig. 4, (a) corresponds to method M_1, with the optimal parameters on the horizontal axis and the entropy on the vertical axis. (b), (c) and (d) correspond to methods M_2, M_3, and M_4, with the optimal parameters on the horizontal axis and the joint entropy on the vertical axis. The curves of the uncorrupted image and the corrupted image using different methods are similar, which implies that it is feasible that the joint entropy replaces the entropy as information similarity measures. The curves in (a) ~ (d), are smooth, have wide capturing ranges, and minima lying in the neutral

parameters ($b_i = e_i = 0$) at which the original image remains unchanged. It is clear that the simulated image degradation process increases the (joint) entropy and, thus the (joint) information of the uncorrupted image. The curve (e)～(h) show that the entropy (or joint entropy) of the original corrupted image is reduced by changing the values of some parameters and transforming the image, which implies that the correction model is capable of reducing the information of a corrupted image.

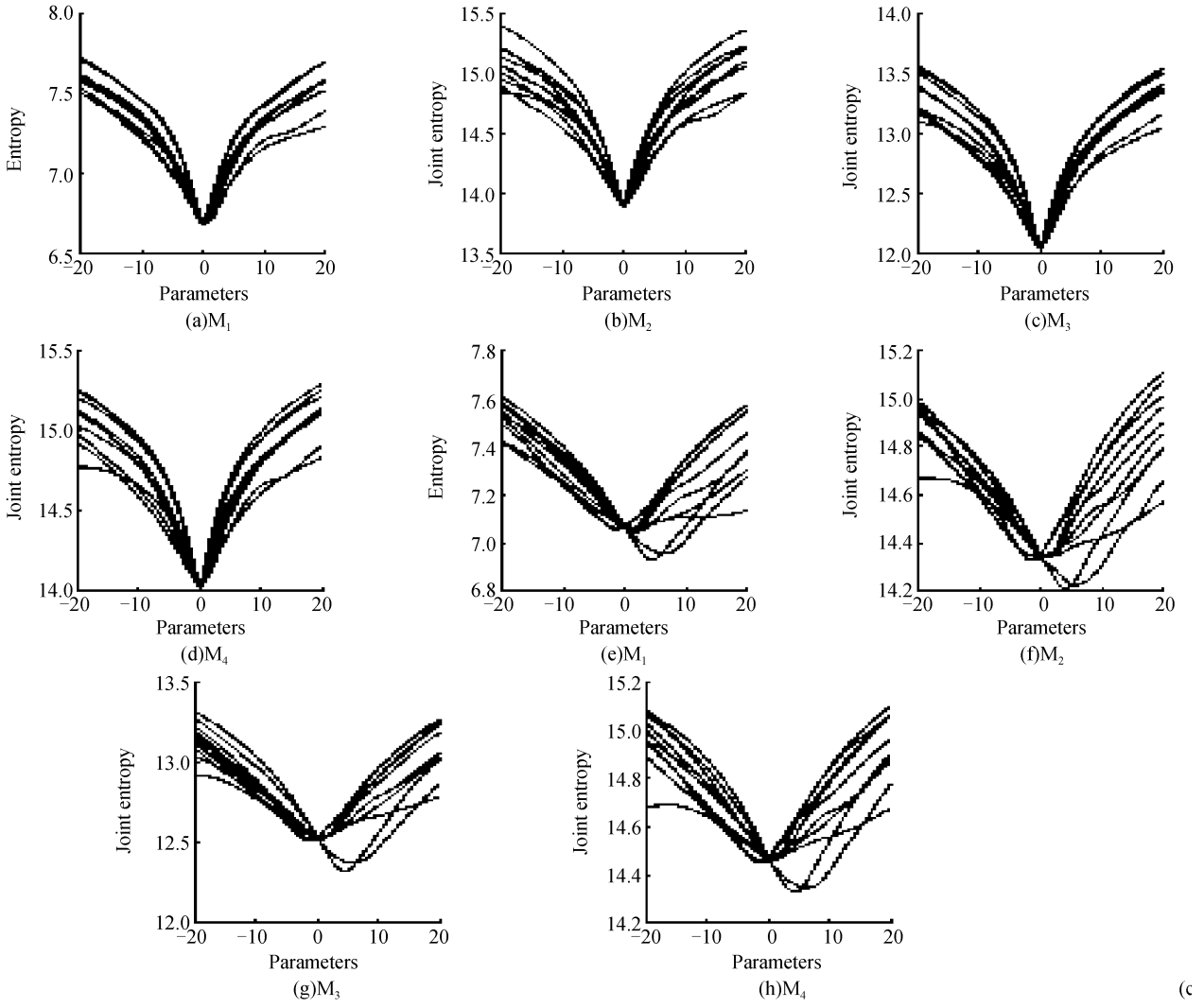

Fig. 4 Comparison of different methods

The corrupted and uncorrupted images come from the BrainWeb Simulated Brain Database[13-14].

2.3 Quantitative evaluation

Quantitative evaluation was performed by computing the coefficient of joint variations (cjv)[9] between gray matter (C_1) and white matter (C_2) of the brain. Cjv is computed from standard deviations σ and mean values μ of the pixel intensities belong to the two matters

$$cjv(C_1, C_2) = \frac{\sigma(C_1) + \sigma(C_2)}{|\mu(C_1) - \mu(C_2)|} \tag{12}$$

Cjv is independent of the changes in contrast and brightness, and measures the intensity inhomogeneity by calculating the degree of intensity overlap between two tissues.

The image set 1, in table 1, were also acquired from the BrainWeb Simulated Brain Database: twelve volumes (four T_1, four T_2, and four PD-weighted) with 3% noise, 181×217×181

Table 1 Coefficient of joint variations (cjv) for image set 1

Volume	cjv_{start} /%	cjv_{M1} /%	cjv_{M2} /%	cjv_{M3} /%	cjv_{M4} /%	cjv_{ideal} /%
T_1 0%	51.6	52.0	51.9	51.8	51.9	51.6
T_2 0%	83.2	82.1	82.8	82.9	82.6	83.2
PD 0%	64.9	64.7	64.7	64.8	64.7	64.9
T_1 40%	69.3	51.6	51.8	51.6	51.7	51.6
T_2 40%	106.4	82.3	82.8	83.1	81.3	83.2
PD 40%	163.0	64.3	64.5	64.7	64.2	64.9
T_1 0% MS	50.9	51.4	51.3	51.1	51.2	50.9
T_2 0% MS	74.9	74.1	74.3	74.7	74.5	74.9
PD 0% MS	66.9	66.7	66.4	66.8	66.7	66.9
T_1 40% MS	68.0	50.8	50.7	50.8	50.8	50.9
T_2 40% MS	123.8	73.7	73.7	74.2	74.0	74.9
PD 40% MS	195.8	66.5	66.5	66.7	66.6	66.9

resolution, 8-bit quantization, and 1 mm slice thickness. Six volumes with 40% and six volumes with 0% inhomogeneity were used, three of each were normal and three with MS lesions. The results of inhomogeneity corrections using the four methods are very close to ideal, but among these four methods, M_3 (second derivative) is the best. cjv_{start}, cjv_{Mi}, and cjv_{ideal} symbolize starting cjv values, final cjv values using method Mi, and ideal cjv values, which are calculated from 0% intensity inhomogeneity, 0% noise nominal images.

Table 2 shows the results on clinical MR volumes of the image set 2, which consists of three volumes (T_1, T_2 and PD; GE Signa Exite 3.0 T), having 512 × 512 × 40 voxels and 8-bit quantization. The white and gray matters are segmented by an interactive intensity based region growing algorithm in the corrected image. All methods can decrease the intensity variations of the white and gray matter and can reduce the overlap of their intensity distributions. On T_2 and PD images, M_3 performs better than other methods. On T_1 images, M_3 performs better than M_1 and M_2, but less than M_4.

Table 2 ***Cjv*** **of gray matter and white matter for real volumes**

Volume	cjv_{start}/%	cjv_{M1}/%	cjv_{M2}/%	cjv_{M3}/%	cjv_{M4}/%
T_1	138.6	127.1	127.0	126.8	125.4
T_2	91.2	88.2	87.5	86.7	87.1
PD	76.3	70.4	69.8	68.6	70.2

3 Discussions and conclusions

The retrospective method, based on modeling the intensity inhomogeneity and minimizing the joint entropy between the acquired images and their derivative images by the parametric polynomial model, was proposed. The method made no assumption on the shape of either the intensity inhomogeneity distribution or the distributions of individual tissues. Section 2.2 shows that the methods do not corrupt the simulated uncorrupted images and can retrospectively correct the simulated corrupted images. In section 2.3, four methods are compared on simulated and clinical MR images. Three variations of the joint information-theoretic methods are implemented, i.e., the M_2, M_3, and M_4 methods, using the joint entropy of image intensities and its first, second, and third derivatives, respectively. The three methods are quantitatively calculated and compared to the M_1 method, the results of which were recently published in[9]. The performances of all methods were expressed by cjv of the gray and white matters. The cjv is invariant to linear intensity inhomogeneity transformations and does not require a complete segmentation. The correction of the simulated images, for which 100% segmentations were available from the web[13], indicated comparable and promising performances of the three joint information-theoretic methods. Of the four methods, the M_3 performed best, which more largely reduces the cjv, and the spreading of gray and white matter distribution. The M_1 method performed less well as it does not consider space information. On real scans, M_3 method outperformed the other methods, except when applied to T1-weighted scans. In such case, the M_4 method was superior.

In general, M_3 performed the best among the methods tested, and the other methods' performances were similar in all modalities. Consequently, the method M_3 is generic method, requires no preprocessing, no parameter setting, and proved to be feasible and efficient.

References

[1] CONDON B R, PATTERSON J, WYPER D, *et al*. Image nonuniformity in magnetic resonance imaging: Its magnitude and methods for its correction[J]. *Br J Radiol*, 1987, **60**(1): 83-87.

[2] SIMMONS A, TOFTS P S, BARKER G J, *et al*. Sources of intensity nonuniformity in spin echo images at 1.5 T[J]. *Magn Reson Med*, 1994, **32**(1): 121-128.

[3] JOHNSON B, ATKINS M S, MACKIEWICH B, *et al*. Segmentation of multiple sclerosis lesions in intensity corrected multispectral MRI[J]. *IEEE Trans Med Imag*, 1996, **15**(4): 154-169.

[4] SLED J G, ZIJDENBOS A P, EVANS A C. A nonparametric method for automatic correction of intensity nonuniformity in MRI data[J]. *IEEE Trans Med Imag*, 1998, **17**(1): 87-97.

[5] WELLS W M III, GRIMSON W E L, JOLESZ F A. Adaptive segmentation of MRI data[J]. *IEEE Trans Med Imag*, 1996, **15**(8): 429-442.

[6] PHAM D L, PRINCE J L. An adaptive fuzzy C-means algorithm for image segmentation in the presence of intensity inhomogeneities[J]. *Pattern Recogn Lett*, 1999, **20**(1): 57-68.

[7] MARGIN J F. Entropy minimization for automatic correction of intensity nonuniformity [A] // IEEE Workshop on Mathematical Methods in Biomedical Image Analysis [C], Washington: IEEE Computer Society, 2000, 162-169.

[8] LIKAR B, MAINTZ B A, VIERGEVER M A, *et al*. Retrospective shading correction based on entropy minimization[J]. *Journal of Microscopy*, 2000, **197**(3): 285-295.

[9] LIKAR B, VIERGEVER M A, PERNUŠ F. Retrospective correction of MR intensity inhomogeneity by information minimization[J]. *IEEE Trans Med Imag*, 2001, **20**(12): 1398-1410.

[10] PLUIM J P W, MAINTZ J B A, VIERGEVER M A. Interpolation artefacts in mutual information-based image registration[J]. *Comput Vis Imag Und*, 2000, **77**(9): 211-

232.
[11] JEFFREY T. Interpolation artifacts in multimodality image registration based on maximization of mutual information[J]. *IEEE Trans on Med Imag*, 2003, **22**(7): 854-864.
[12] STUDHOLME C, HILL D L G, HAWKES D J. An overlap invariant entropy measure of 3D medical image alignment[J]. *Pattern Recognition*, 1999, **32**(1): 71-86.
[13] McConnell Brain Imaging Centre Montreal Neurological Institute, McGill University. BrainWeb: simulated brain database[DB/OL], (2006-06-08) [2006-07-29]. http://www.bic.mni.mcgill.ca/brainweb.
[14] COCOSCO C A, KOLLOKIAN V, KWAN R K S, *et al*. Online interface to a 3-D MRI simulated brain database[J]. *NeuroImage*, 1997, **5**(4): 425.
[15] ZHENG Gang, JIA Zhen-hong. Application of homomorphic technology in infrared images processing[J]. *Acta Photonica Sinica*, 2005, **34**(9): 1401-1403.
[16] NIU Jian-jun, LIU Shang-qian, YAO Rong-hui, *et al*. Algorithm for image correction in high precision imaging measurement system[J]. *Acta Photonica Sinica*, 2006, **35**(9): 1317-1320.
[17] XU Tian-hua, ZHAO Yi-gong. Iterative least square-based algorithm for nonuniformity correction of infrared focal plane arrays[J]. *Acta Photonica Sinica*, 2006, **35**(2): 261-264.
[18] LI Xiang, LUO Shu-qian. Bias field correction based tissue classification of MR images of brain[J]. *Beijing Biomedical Engineering*, 1998, **17**(3): 129-135.
[19] LI Yin, WANG Ze, ZHU Yi-sheng. An improved homomorphic filtering method for inhomogeneity correction of magnetic resonance images [J]. *Journal of Shanghai Jiaotong University*, 2003, **37**(9): 1452-1455.
[20] ZHOU Jin-mei, XING Ting-wen, LIN Wu-mei. Precision analysis of nonuniformity correction of IRFPA [J]. *Acta Photonica Sinica*, 2005, **34**(11): 1681-1684.

基于灰度和空间联合信息最小化的磁共振图像偏差场纠正

刘常春[1], 胡顺波[1,2], 顾建军[1,3], 杨金宝[1]
(1 山东大学 控制科学与工程学院, 山东 济南 250061)
(2 临沂师范学院 物理系, 山东 临沂 276005)
(3 达尔豪西大学 电气与计算机工程系, 哈利法克斯, 加拿大)
收稿日期: 2007-01-09

摘 要: 在磁共振图像(MR)的偏差场纠正中, 针对灰度信息最小化方法没有考虑空间信息问题, 提出联合信息最小化方法, 该方法把图像的灰度信息和空间信息结合起来. 空间信息采用灰度导数信息. 被偏差场破坏的图像灰度及其导数值的联合信息(联合熵)大于对应的没被偏差场破坏的图像联合熵. 联合熵是通过计算灰度及其导数值的联合概率分布得到. 仿真脑部 MR 数据和临床脑部 MR 数据的试验结果都表明, 灰度及其二阶导数联合信息最小化方法纠正效果良好, 大大减少了脑白质和脑灰质的灰度交叠.
关键词: 图像处理; 偏差场纠正; 磁共振成像; 联合熵最小化

LIU Chang-chun was born in 1959. He received M. S. degree from Shandong University in 1982. Now he is professor in Shandong University. His main research interests are in the field of biomedical engineering.